



vehicle based on an SNN, which relies solely on the sensory feedback provided by an airborne radar. We successfully demonstrate the performance of the radar-based neurocontroller onboard the aerial platform in real-world experiments, quantitatively comparing the results with those of an ANN and a proportional-integral-derivative (PID) controllers. Second, we propose the design of an open-source, low-cost, lightweight blimp platform with a 3D printable gondola, that allows for the inclusion of custom sensors and actuators. This facilitates its replication and customization for different applications. The remainder of the paper is organized as follows: Section II provides an overview of the state-of-the-art in micro-airship design and spiking flight neurocontrollers. Afterwards, in Section III, we present the proposed MAV design, introduce the altitude control approach based on the airborne radar, the structure of the SNN controller, the evolutionary strategy for training the network, and a blimp computational model to perform the training in a simulated environment. Then, in Section IV, we describe the real-world experimental setup as well as discuss the obtained results. Finally, Section V concludes the work and delineates future research directions.

## II. RELATED WORK

### A. Micro-airship Design

Even though the golden era of giant cargo airships has faded, the advantages offered by lighter-than-air crafts prevail. Blimps are, slowly but surely, attracting increasing interest in the realm of unmanned aerial vehicles [17, 18]. They present endless possibilities in terms of their design. For example in [19], a three-propeller, low-cost platform is presented that is equipped with a camera and a compact, but closed-configuration gondola. An alternative design is proposed in [20], where the authors introduce a novel actuation mechanism based on two propellers mounted on a rotating shaft, which is oriented using a servomotor. Other examples of higher complexity include [21–23]. Although these alternatives have proven successful for their specific applications, they lack the versatility that can be achieved by leaving room for incorporating additional sensors and/or actuators. Besides, only [19] is open-source and lightweight enough to be mounted on commercially available blimp balloons. For the purpose of clear comparison, the main contributions of the state-of-the-art and our approach are summarized in Table I.

TABLE I  
COMPARISON BETWEEN THE DIFFERENT BLIMP DESIGNS

Property	[19]	[20]	[21]	[22]	[23]	Ours
Easily customizable gondola	-	✓	-	-	-	✓
Low-cost design	✓	✓	✓	✓	-	✓
Open-source availability	✓	-	-	-	-	✓
Lightweight Microfoil blimp	✓	-	-	-	-	✓
Number of propellers	3	2	4	6	4	2
Number of servomotors	-	1	-	3	-	1

### B. Spiking Neural Network-based MAV Control

The inherent nonlinear dynamics of most MAVs makes them challenging to control. Moreover, their restrictive weight constraints inevitably limit the computational power of the controller. SNNs enable computing with highly parallel architectures made of simple integrate-and-fire neurons interconnected by weighted synapses. Implementations of spiking flight neurocontrollers include [24], where the authors propose an SNN for robust control of a simulated quadrotor in challenging wind conditions. They achieve a better performance in waypoint holding experiments compared with a hand-tuned PID and a multi-layer perceptron network. Another example is presented in [25], where an SNN controller that adapts online to control the position and orientation of a flapping drone is proposed. SNNs have also been applied to obstacle avoidance tasks, as direct flight [11] or decision-making [26] controllers. In both cases they use reward-modulated learning rules for training the SNN. Although these MAV controllers have excelled in simulated environments, their main limitation is that they have not been evaluated in real-world experiments. The scope of works that have implemented SNN controllers for MAVs in real scenarios is much more limited. The first work that integrates an SNN in the closed-loop control of a real-world flying robot is very recent [27]. There, the authors present an SNN for controlling the landing of a quadrotor by exploiting the optical flow divergence from a downward-looking camera and the readings of an inertial measurement unit (IMU). To address the learning problem of SNNs [28], they adopt an evolutionary training strategy. In [29], this controller is enhanced by using hardware specifically designed for neuromorphic applications. Although not tested in free flight experiments, the potential advantages of SNN controllers implemented in these devices are also demonstrated in [30]. Our work aims to extend the framework proposed in [27], by (1) controlling the altitude instead of landing; (2) considering an open-source micro blimp, which has less control authority and harder to model dynamics than a quadrotor; and (3) exploiting solely the range measurements provided by a radar, reducing the number of required sensors on-board.

## III. METHODOLOGY

### A. Open-source Micro-airship

The proposed design for the micro autonomous airship is illustrated in Fig. 2. The reader interested in replicating the platform can find further details, links to re-sellers, prices, and parts for 3D printing at: [https://github.com/tudelft/blimp\\_snn](https://github.com/tudelft/blimp_snn). The airship’s gondola can be 3D printed and assembled in a modular fashion, with a total frame weight of just 9g. Due to its open configuration, the components mounted on the gondola can be easily interchanged, leaving room for versatility on the selection of sensors and actuators. In addition, we include a rotary shaft with a case for accommodating the propellers on both ends for controlling the altitude. Finally, we incorporate four hitches on top of the gondola, where we tape Velcro

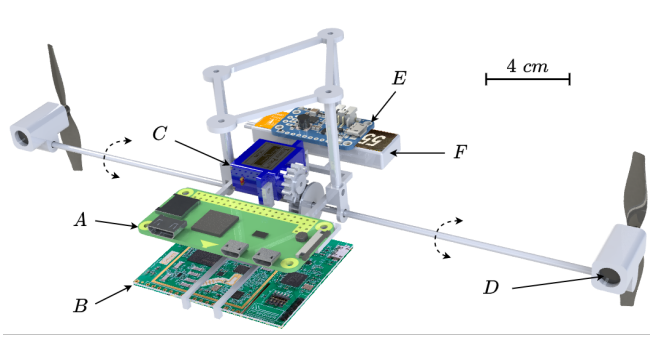


Fig. 2. Proposed airship design. (A) Raspberry Pi W Zero; (B) 24 GHz Infineon Radar Position2Go; (C) Sub-micro Servo SG51R; (D) 8520 Coreless Motor; (E) PowerBoost 500 Basic; (F) 550mA 3.8V Li-Po battery.

strips for attaching the envelope. Regarding the electronic components, we use a Raspberry Pi W Zero as the central communication and control unit, running the Raspbian Lite operating system. The robot’s steering is achieved through the micro servomotor mounted on the gondola and the two core-less direct current (DC) motors attached at each end of the shaft. Specifically, the servo is responsible for the rotation of the shaft, up to  $180^\circ$ , and the DC motors allow for an independent control of the thrust on each side. Additional peripheral components include a step-up voltage regulator, a 500 mAh Li-Po battery and a motor driver. Finally, a fast chirp frequency-modulated continuous wave (FMCW) radar module from Infineon with a resolution of  $\pm 20$  cm is used as a ranging sensor for the closed-loop control. Concerning the airship’s envelope, the material chosen is Microfoil due to its excellent gas retention capabilities [19]. We select a model that provides the largest achievable payload among the commercially available miniature blimps (150g) while keeping a relatively low price. For our application, we use helium as the lifting gas. Considering all the aforementioned elements, the proposed platform weights a total of 147g. To integrate the different components and perform the computations on-board we adopt the Robot Operating System (ROS) [31] framework. In addition, a teleoperation package to manually control the airship from a ground computer keyboard via a secure shell (SSH) connection is also provided in the repository included at the beginning of this section.

### B. Altitude Controllers

In order to control the airship’s altitude, the commands are provided in terms of motor voltages,  $u \in [-u_{\max}, u_{\max}]$  [V], with  $u_{\max} = 3.3$  [V]. The larger the absolute value of  $u$ , the more thrust the propellers provide, and therefore, the greater the acceleration of the blimp will be. When  $u > 0$ , the robot moves upwards and, when  $u < 0$ , the robot moves downwards, with the shaft rotated  $180^\circ$ . To determine the required control actions for tracking an arbitrary reference altitude  $h_{\text{ref}}$ , we process the readings from the radar to get an estimate of the current altitude  $h_{\text{curr}}$  of the blimp [32] – the range-Doppler algorithm [33], along with a median filter, is used to estimate the altitude. Then, to effectively track an arbitrary altitude command, we design a controller that

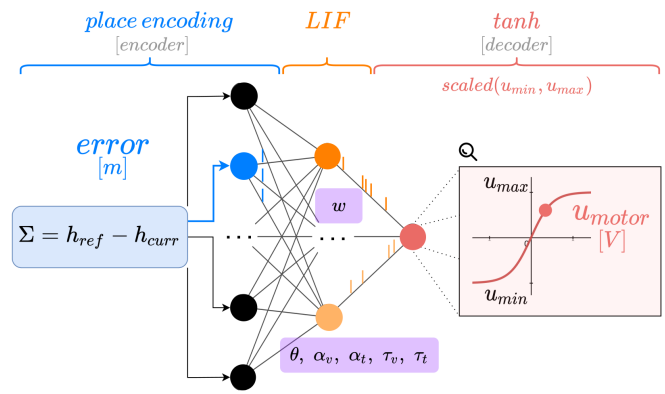


Fig. 3. Schematic of the SNN controller architecture. The (evolved) network parameters are highlighted in violet, being  $w$  the synaptic weights,  $\theta$  the spiking threshold,  $\alpha_{v/t}$  the scaling constant for the increase of the voltage/trace by a single spike, and  $\tau_{v/t}$  the decay for the voltage/trace.

provides a mapping between the altitude error,  $h_{\text{ref}} - h_{\text{curr}}$ , and the motor voltages,  $u$ , such that the former is minimized. We consider three distinct approaches for benchmarking purposes: a linear PID, an artificial neural network, and a spiking neural network.

1) *PID controller*: A conventional PID is one of the most simple, yet widespread methods for addressing control problems. In discrete form, the mapping between the error signal  $e_k = h_{\text{ref}}(k) - h_{\text{curr}}(k)$  and the motor command  $u_k$  is given by [34]:

$$u_k = K_p e_k + \frac{K_d}{T} (e_k - e_{k-1}) + K_i T (e_k + e_{k-1}) \quad (1)$$

where  $K_p$ ,  $K_i$  and  $K_d$  refer to the proportional, integral and derivative gains, respectively,  $T$  to the sampling period, and  $k$  to the timestamp. These are tuned empirically using the proposed MAV platform.

2) *ANN controller*: We propose a standard, non-neuromorphic ANN controller where the tracking error  $h_{\text{ref}} - h_{\text{curr}}$  is directly fed into the network in the form of a continuous signal. The network consists of a single neuron in the first and last layers, and two hidden layers containing 3 and 2 neurons respectively. The input and the two hidden layers operate with a  $\tanh()$  activation function. At the output layer, a linear neuron provides the value of the motor command  $u$ , clamped to the interval  $\pm u_{\max}$  [V].

3) *SNN controller*: The proposed SNN architecture is illustrated in Fig. 3: it consists of three fully connected layers (10 – 5 – 1 neurons). The input layer encodes the altitude error signal into spikes using position coding: the input values of  $h_{\text{ref}} - h_{\text{curr}}$  are divided into 10 intervals, with each of them assigned to a different neuron. The first and last intervals corresponds to  $]-\infty, -0.4[$  and  $]0.4, \infty[$ , respectively, while the range of the remainder 8 neurons is uniformly distributed between  $[-0.4, 0.4]$ . Each time the altitude error falls within one of these intervals, the corresponding neuron fires a single spike. The hidden layer consists of five leaky integrate-and-fire (LIF) neurons, where the membrane potential of the  $i$ -th

neuron,  $v_i(t)$ , is governed by the following equation:

$$v_i(t) = \tau_{v_i} \cdot v_i(t - \Delta t) + \alpha_{v_i} u_i(t) \quad i = 1, \dots, 5 \quad (2)$$

referring  $\tau_{v_i} \in [0, 1]$  to the decay factor per time-step  $\Delta t$ ,  $\alpha_{v_i}$  to a scaling constant, and  $u_i(t)$  to the synaptic input current:

$$u_i(t) = \sum_{j=1}^{10} w_{ij} s_j(t). \quad (3)$$

that is, multiplying the incoming spikes from the  $j$ -th input neuron  $s_j(t)$ , by the synaptic weights  $w_{ij}$ . Whenever the membrane potential  $v_i(t)$ , reaches a certain threshold  $\theta_i$ , a postsynaptic spike is triggered and  $v_i(t)$  resets back to 0. The output layer decodes the spikes back into a real value. It consists of a single non-spiking neuron with a scaled  $\tanh()$  activation function. The neuron conducts a weighted sum of the so-called spike traces,  $X_i(t)$ , which acts as a low-pass filter with decay  $\tau_i \in [0, 1]$ , and is computed as:

$$X_i(t) = \tau_i \cdot X_i(t - \Delta t) + \alpha_i s_i(t), \quad (4)$$

being the definition of  $\tau_i$  and  $\alpha_i$  analogous to  $\tau_{v_i}$  and  $\alpha_{v_i}$ . The resulting value is scaled within the control limits,  $\pm u_{\max}$ . Following this, the motor command,  $u$ , is given by:

$$u(t) = u_{\max} \cdot \tanh \left( \sum_{i=1}^5 w_i X_i(t) \right) \quad (5)$$

### C. Evolutionary Framework

For training the neural controllers we adopt an evolutionary strategy with a mutation-only procedure. Each evolution begins with a randomly initialized population of  $N$  individuals. The offspring is obtained by performing a randomized tournament selection of  $M$  individuals, i.e., randomly selecting  $M$  aspirants from the population and keeping the one with the best fitness. This is repeated  $N$  times, so that the population size is invariant. The  $n$ -th individual is mutated with a probability of  $p_{mut}^{(n)} = 0.4$ , and its  $m$ -th parameter with  $p_{mut}^{(m)} = 0.6$ . These mutations take place according to uniform probability distributions  $\mathcal{U}\{\cdot, \cdot\}$ , whose range is shown in Table II for both the SNN and ANN. For the latter, the open parameters are the biases,  $b_i$ , and analogously to SNNs, the weights,  $w_{ij}$ .

TABLE II  
PARAMETERS MUTATED DURING EVOLUTION

	Parameter	Domain	Mutation
SNN	$w_{ij}$	$[-5, \dots, 5]$	$\mathcal{U}\{-2.5, 2.5\}$
	$\theta_i, \tau_{v_i}, \tau_i$	$[0, \dots, 1]$	$\mathcal{U}\{-0.5, 0.5\}$
	$\alpha_{v_i}, \alpha_i$	$[0, \dots, 2]$	$\mathcal{U}\{-1.0, 1.0\}$
ANN	$w_{ij}, b_i$	$[-5, \dots, 5]$	$\mathcal{U}\{-2.5, 2.5\}$

The mutated offspring is then evaluated in a model-based simulation environment (see Section III-D), where a source of random Gaussian noise is added to the radar signal. Since this randomization stimulates the persistence of controllers that are independent of such disturbances, it helps minimizing the reality gap [35]. During the evaluation,

a set of 10 different reference altitudes  $h_{ref} \in [0, 3]$  is provided along a total simulated duration of  $T = 15$  seconds each. The fitness of each individual is then quantified as the root mean squared altitude error (RMSAE):

$$\text{RMSAE} = \sqrt{\frac{1}{T} \sum_{k=0}^T (h_{ref}(k) - h_{curr}(k))^2} \quad (6)$$

During the evolution process, a *hall of fame* which holds the 5 best performing individuals across all generations, is maintained. This prevents discarding those who have achieved a good performance. After  $N_{gen}$  generations, the individuals are also reevaluated on five more random sets of altitudes to increase the robustness. The best-performing ones are selected for further real-world experiments. The architecture of the neural controllers is kept fixed during the evolution. The choice for a specific network architecture is made experimentally, after repeating this training process several times for networks of different complexities. Concretely, the simplest and smallest network which does not compromise the control performance is selected.

### D. Model-based Simulation Environment

The altitude controllers evolve in a simulated environment since it would be infeasible to perform all the required evaluations in the real world. For that, we develop a dynamical model of the blimp to obtain a mapping between the motor commands and the evolution of the blimp's altitude over time. To simplify the training and avoid adding further complexity, we consider a linear model. We assume that the acceleration at the  $k$ -th time step  $\ddot{h}_k$ , is proportional to the voltage applied to the motors,  $u$ , i.e.

$$\ddot{h}_k = a_1 u_{k-1} + a_2 u_{k-2} \quad (7)$$

where  $a_i$  is the proportionality constant for the motor command at time instant  $k - i$ . However, since the acceleration cannot be directly measured with the radar sensor, we can instead express this relation in terms of the measured altitude,  $h$  by taking Euler's discretization of the derivative. Applying the Z-transform, we obtain the following transfer function, which maps the commands  $u_k$  to the altitude  $h_k$ :

$$h_k = \frac{a_1 z^{-1} + a_2 z^{-2}}{1 - 2z^{-1} + z^{-2}} u_k \quad (8)$$

To determine the unknown parameters  $a_i$ , we collect a data-set by tele-operating the blimp and measuring its altitude over time. After subtracting the mean, we infer the model parameters by minimizing the normalized root mean squared altitude error (NRMSAE), which can be interpreted as a measure of how well the expected response  $h_k$  matches the observed data  $\hat{h}_k$ .

## IV. RESULTS

### A. Experimental Setup

1) *Simulation*: To train the neural controllers, we evolved five randomly initialized populations of 100 individuals through 300 generations, following the procedure described

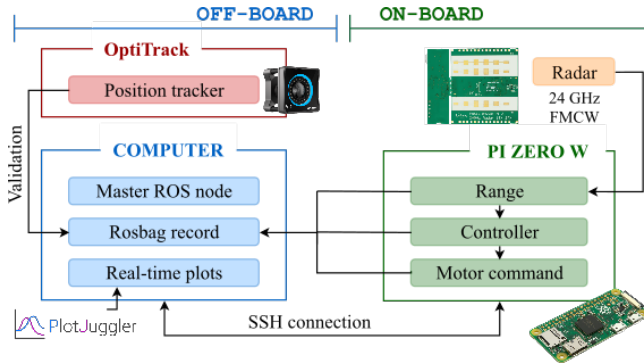


Fig. 4. System overview. After processing the feedback provided by the radar sensor, an estimate of the range is sent to the Raspberry Pi Zero W control unit. Only data recording and real-time plotting operations are conducted on the ground computer, which communicates with the Pi via an SSH connection. The OptiTrack is used during the post-processing stage just for validation purposes.

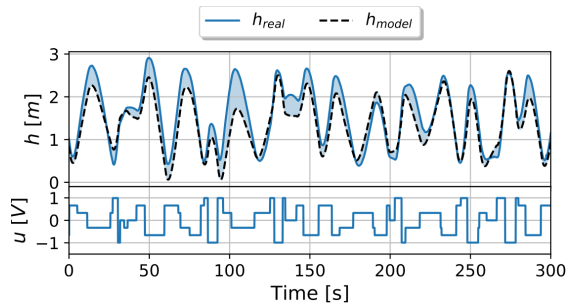


Fig. 5. Validation of the blimp model. **Bottom:** Motor commands. **Top:** The ground truth evolution of the altitude,  $h_{real}$ , compared with the evolution predicted by the model,  $h_{model}$ . The error is represented by the blue area.

in Section III-C. The implementation of the evolutionary optimization is based on the Distributed Evolutionary Algorithms in Python (DEAP) [36] framework, while the simulation of the networks is performed by means of the PySNN library [37].

2) *Real-World:* An overview of the setup is shown in Fig. 4. The on-board control unit is a 1GHz single-core processor Raspberry Pi Zero W with 512MB RAM. The Infineon Position2Go radar provides altitude measurements. The control loop runs at a rate of 5 Hz.

### B. Blimp Model

Following the procedure explained in Section III-D, we infer the parameters of a blimp model of the form (8), based on experimental data gathered using the real hardware. In Fig. 5 we show a comparison between the evolution of the altitude predicted by the model and the ground truth when applying identical motor commands. We can see that we are able to reproduce the blimp’s behavior using the proposed data-driven model, with a RMSAE of 0.27m over the 300 seconds run.

### C. Controller Evaluation

We evaluate the performance of three different altitude controllers based on a linear PID, an ANN, and an SNN. The

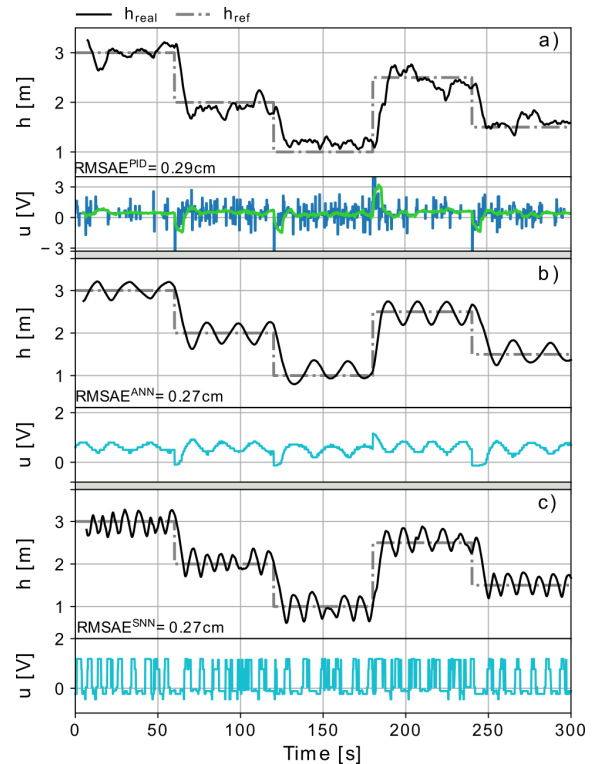


Fig. 6. Experimental evaluation of the considered controllers. For all three sub-figures, at the bottom we have the motor commands, and on top, the evolution of the blimp’s altitude  $h_{real}$  compared with the reference  $h_{ref}$ . (a) PID. (b) ANN. (c) SNN.

tracking precision is tested on a sequence of five different way-points  $h_d = \{3, 2, 1, 2.5, 1.5\}$ m, maintained during 60s.

1) *PID controller:* The experimental results are depicted in Fig. 6(a). We can see that we can track the altitude commands effectively. Quantitatively, we obtain a RMSAE of 0.29m, which indicates a satisfactory performance, considering that the uncertainty of the radar sensor is of  $\pm 0.2$ m.

2) *ANN controller:* The obtained results are shown in Fig. 6(b). We can see that the blimp effectively converges to the altitude set-point but presents an oscillatory behavior. This is mainly because of two reasons: the minor contribution of the diminished discrepancies between the model and the vehicle’s inherent dynamics; and the slow responsiveness of the system, especially when the motor commands are not too abrupt, as it is the case. However, it can be noted that the trajectory is smoother than with a PID. The RMSAE now corresponds to 0.27m.

3) *SNN controller:* The experimental results for this case are displayed in Fig. 6(c). We note that the behavior and performance are similar to the ANN case, but with faster oscillations, due to the output’s binary nature caused by the presence or absence of the spike. The RMSAE is of 0.27m.

## V. CONCLUSION

In this paper, we aim at paving the way toward fully neuromorphic control for flying vehicles. The results obtained in real-world experiments successfully demonstrate the system’s performance. By comparing it with a standard

PID and an artificial neural network, we corroborate the advantages offered by SNNs in terms of adaptability and low control effort – ultimately, the use of SNNs on-board neuromorphic controllers such as the Loihi [38] will fully demonstrate their advantages in terms of processing time and energy, while helping closing the loop towards a fully neuromorphic control of robotic systems.

## REFERENCES

- [1] Y. Jiang, C. Yang, J. Na, G. Li, Y. Li, and J. Zhong, “A brief review of neural networks based learning and control and their applications for robots,” *Complexity*, Oct 2017.
- [2] O. I. Abiodun, A. Jantan, A. E. Omolara, K. V. Dada, N. A. Mohamed, and H. Arshad, “State-of-the-art in artificial neural network applications: A survey,” *Heliyon*, vol. 4, no. 11, 2018.
- [3] B. Kusumoputro, H. Suprijono, M. A. Heryanto, and B. Y. Suprpto, “Development of an attitude control system of a heavy-lift helicopter using elman recurrent neural networks,” in *2016 22nd International Conference on Automation and Computing (ICAC)*, 2016, pp. 27–31.
- [4] H. Suprijono and B. Putro, “Direct inverse control based on neural network for unmanned small helicopter attitude and altitude control,” *Journal of Telecommunication, Electronic and Computer Engineering*, vol. 9, pp. 99–102, 2017.
- [5] M. Heryanto, H. Suprijono, B. Suprpto, and B. Putro, “Attitude and altitude control of a quadcopter using neural network based direct inverse control scheme,” *Advanced Science Letters*, vol. 23, no. 5, pp. 4060–4064, May 2017.
- [6] A. Yousefzadeh, S. Hosseini, P. Holanda, S. Leroux, T. Werner, T. Serrano-Gotarredona, B. L. Barranco, B. Dhoedt, and P. Simoens, “Conversion of synchronous artificial neural network to asynchronous spiking neural network using sigma-delta quantization,” in *2019 IEEE International Conference on Artificial Intelligence Circuits and Systems (AICAS)*, 2019, pp. 81–85.
- [7] W. Maas, “Networks of spiking neurons: The third generation of neural network models,” *Trans. Soc. Comput. Simul. Int.*, vol. 14, no. 4, p. 1659–1671, Dec. 1997.
- [8] J. H. Lee, T. Delbruck, and M. Pfeiffer, “Training deep spiking neural networks using backpropagation,” *Frontiers in Neuroscience*, vol. 10, p. 508, 2016.
- [9] M. Davies, N. Srinivasa, T.-H. Lin, G. China, Y. Cao, S. H. Choday, G. Dimou, P. Joshi, N. Imam, S. Jain, Y. Liao, C.-K. Lin, A. Lines, R. Liu, D. Mathiakutty, S. McCoy, A. Paul, J. Tse, G. Venkataramanan, Y.-H. Weng, A. Wild, Y. Yang, and H. Wang, “Loihi: A neuromorphic manycore processor with on-chip learning,” *IEEE Micro*, vol. 38, no. 1, pp. 82–99, 2018.
- [10] J. Stuijt, M. Sifalakis, A. Yousefzadeh, and F. Corradi, “ $\mu$ Brain: An Event-Driven and Fully Synthesizable Architecture for Spiking Neural Networks,” *Frontiers in Neuroscience*, vol. 15, p. 538, 2021.
- [11] G. Foderaro, C. Henriquez, and S. Ferrari, “Indirect training of a spiking neural network for flight control via spike-timing-dependent synaptic plasticity,” in *49th IEEE Conference on Decision and Control (CDC)*, 2010, pp. 911–917.
- [12] N. Mathew, S. L. Smith, and S. L. Waslander, “Planning paths for package delivery in heterogeneous multirobot teams,” *IEEE Transactions on Automation Science and Engineering*, vol. 12, no. 4, pp. 1298–1308, 2015.
- [13] B. Arbanas, A. Ivanovic, M. Car, T. Haus, M. Orsag, T. Petrovic, and S. Bogdan, “Aerial-ground robotic system for autonomous delivery tasks,” in *2016 IEEE International Conference on Robotics and Automation (ICRA)*, 2016, pp. 5463–5468.
- [14] G. de Croon, H. Ho, C. D. Wagter, E. van Kampen, B. Remes, and Q. Chu, “Optic-flow based slope estimation for autonomous landing,” *International Journal of Micro Air Vehicles*, vol. 5, no. 4, pp. 287–297, 2013.
- [15] A. Borowczyk, D.-T. Nguyen, A. Phu-Van Nguyen, D. Q. Nguyen, D. Saussié, and J. L. Ny, “Autonomous landing of a multirotor micro air vehicle on a high velocity ground vehicle\*\*this work was partially supported by cfi jelf award 32848 and a hardware donation from dji.” *IFAC-PapersOnLine*, vol. 50, no. 1, pp. 10488–10494, 2017, 20th IFAC World Congress.
- [16] Y. Li, M. Nahon, and I. Sharf, “Airship dynamics modeling: A literature review,” *Progress in Aerospace Sciences*, vol. 47, no. 3, pp. 217 – 239, 2011.
- [17] P. G. Artaxo, A. Bourgois, H. Sardinha, H. Vieira, E. C. de Paiva, A. R. Fioravanti, and P. A. Vargas, “Autonomous cooperative flight control for airship swarms,” 2020.
- [18] E. Price, Y. T. Liu, M. J. Black, and A. Ahmad, “Simulation and control of deformable autonomous airships in turbulent wind,” 2020.
- [19] G. Gorjup and M. Liarokapis, “A low-cost, open-source, robotic airship for education and research,” *IEEE Access*, vol. 8, pp. 70713–70721, 2020.
- [20] S. U. Ferdous, A. Mohammadi, and S. Lakshmanan, “Developing a low-cost autonomous blimp with a reduced number of actuators,” in *Unmanned Systems Technology XXI*, C. M. Shoemaker, H. G. Nguyen, and P. L. Muench, Eds., vol. 11021, International Society for Optics and Photonics. SPIE, 2019, pp. 73 – 80.
- [21] K. Watanabe, N. Okamura, and I. Nagai, “Closed-loop control experiments for a blimp robot consisting of four-divided envelopes,” in *IECON 2015 - 41st Annual Conference of the IEEE Industrial Electronics Society*, 2015, pp. 2568–2573.
- [22] S. Oh, S. Kang, K. Lee, S. Ahn, and E. Kim, “Flying display: Autonomous blimp with real-time visual tracking and image projection,” in *2006 IEEE/RSJ International Conference on Intelligent Robots and Systems*, 2006, pp. 131–136.
- [23] M. Burri, L. Gasser, M. Käch, M. Krebs, S. Laube, A. Ledergerber, D. Meier, R. Michaud, L. Mosimann, L. Müri, C. Ruch, A. Schaffner, N. Vuilliomonet, J. Weichart, K. Rudin, S. Leutenegger, J. Alonso-Mora, R. Siegwart, and P. Beardsley, “Design and control of a spherical omnidirectional blimp,” in *2013 IEEE/RSJ International Conference on Intelligent Robots and Systems*, 2013, pp. 1873–1879.
- [24] D. Howard and A. Elfes, “Evolving spiking networks for turbulence-tolerant quadrotor control,” *Artificial Life Conference Proceedings*, no. 26, pp. 431–438, 2014.
- [25] T. S. Clawson, S. Ferrari, S. B. Fuller, and R. J. Wood, “Spiking neural network (snn) control of a flapping insect-scale robot,” in *2016 IEEE 55th Conference on Decision and Control (CDC)*, 2016, pp. 3381–3388.
- [26] F. Zhao, Y. Zeng, and B. Xu, “A brain-inspired decision-making spiking neural network and its application in unmanned aerial vehicle,” *Frontiers in Neurobotics*, vol. 12, p. 56, 2018.
- [27] J. J. Hagenaars, F. Paredes-Valles, S. M. Bohte, and G. C. H. E. de Croon, “Evolved neuromorphic control for high speed divergence-based landings of mavs,” *IEEE Robotics and Automation Letters*, vol. 5, no. 4, p. 6239–6246, Oct 2020.
- [28] X. Wang, X. Lin, and X. Dang, “Supervised learning in spiking neural networks: A review of algorithms and evaluations,” *Neural Networks*, vol. 125, pp. 258–280, 2020.
- [29] J. Dupeyroux, J. J. Hagenaars, F. Paredes-Vallés, and G. de Croon, “Neuromorphic control for optic-flow-based landings of mavs using the loihi processor,” *CoRR*, vol. abs/2011.00534, 2020.
- [30] A. Vitale, A. Renner, C. Nauer, D. Scaramuzza, and Y. Sandamirskaya, “Event-driven vision and control for uavs on a neuromorphic chip,” in *IEEE International Conference on Robotics and Automation (ICRA)*, 2021.
- [31] M. Quigley, K. Conley, B. P. Gerkey, J. Faust, T. Foote, J. Leibs, R. Wheeler, and A. Y. Ng, “Ros: an open-source robot operating system,” in *ICRA Workshop on Open Source Software*, 2009.
- [32] N. Wessendorp, R. Dinaux, J. Dupeyroux, and G. de Croon, “Obstacle avoidance onboard mavs using a fmcw radar,” 2021.
- [33] V. Winkler, “Range doppler detection for automotive fmcw radars,” *2007 European Radar Conference*, pp. 166–169, 2007.
- [34] K. Ogata, *Discrete-Time Control Systems*. USA: Prentice-Hall, Inc., 1987.
- [35] K. Y. Scheper and G. C. de Croon, “Evolution of robust high speed optical-flow-based landing for autonomous mavs,” *Robotics and Autonomous Systems*, vol. 124, p. 103380, 2020.
- [36] F.-A. Fortin, F.-M. D. Rainville, M.-A. Gardner, M. Parizeau, and C. Gagné, “Deep: Evolutionary algorithms made easy,” *Journal of Machine Learning Research*, vol. 13, no. 70, pp. 2171–2175, 2012.
- [37] B. Büller, “Pysnn,” <https://github.com/BasBuller/Pysnn>, 2019.
- [38] M. Davies, N. Srinivasa, T. Lin, G. China, Y. Cao, S. H. Choday, G. Dimou, P. Joshi, N. Imam, S. Jain, Y. Liao, C. Lin, A. Lines, R. Liu, D. Mathiakutty, S. McCoy, A. Paul, J. Tse, G. Venkataramanan, Y. Weng, A. Wild, Y. Yang, and H. Wang, “Loihi: A neuromorphic manycore processor with on-chip learning,” *IEEE Micro*, vol. 38, no. 1, pp. 82–99, 2018.